FOREX Publication
Open Access | Rapid and quality publishing

International Journal of
Electrical and Electronics Research (IJEER)
Research Article | Volume 10, Issue 4 | Pages 811-816 | e-ISSN: 2347-470X

Modelling and Performance Analysis of CuPc and C60 Based Bilayer Organic Photodetector

Gazia Manzoor[1], Kamal Kant Sharma[2], Gaurav Kumar Bharti[3*] and Debarati Nath[4]

[1,2,3]Department of Electrical Engineering, Chandigarh University, Mohali, Punjab, India, [1]ergaziaqadri@gmail.com, [2]kamalkant.ee@cumail.in, [3]gaurav.e11977@cumail.in
[4]Department of Electronics and Communication Engineering, Chandigarh University, Mohali, Punjab, India, debaratiphd@gmail.com

***Correspondence:** Gaurav Kumar Bharti; gaurav.e11977@cumail.in

ABSTRACT- An optoelectronic device model for organic photodetector based on bilayer structure has been presented. Drift-diffusion and optical-generation model from Synopsys tool have been incorporated and its optoelectronics behavior has been discussed. The model shows an outstanding rectifying behavior under dark condition due to the different work function of the electrodes. Photocurrent density of 6.64 mA/cm^2 is found under the illumination of 3 W/cm^2. To analyze rectifying behavior of current density-voltage characteristics of the organic photodetector, the curve has been fitted with the Shockley equation. The enhancement of ideality factor of diode current under illumination from that of dark current at forward bias is attributed to enhancement of recombination loss due to generation of photo-carrier and injection of carriers from electrodes. Almost equal probability of photocurrent spectra in the entire spectral region indicates equal probability of exciton generated and dissociated at the interface between CuPc and C_{60} layers. The detectivity of the proposed photodetector is calculated and it is in order of 10^{10} Jones at 650 nm due to high dark current density and recombination loss. The presence of interface trap density and large transport distance give evidence of low response speed in the device.

General Terms: Modelling, Optoelectronic Devices, Photodetector.
Keywords: Photodetector, Organic Photodetector, Device, Simulation and Modelling.

ARTICLE INFORMATION
Author(s): Gazia Manzoor, Kamal Kant Sharma, Gaurav Kumar Bharti and Debarati Nath;
Received: 17/06/2022; **Accepted**: 01/10/2022; **Published**: 18/10/2022;
e-ISSN: 2347-470X;
Paper Id: IJEER-RDEC2009;
Citation: 10.37391/IJEER.100408
Webpage-link:
https://ijeer.forexjournal.co.in/archive/volume-10/ijeer-100408.html

Publisher's Note: FOREX Publication stays neutral with regard to Jurisdictional claims in Published maps and institutional affiliations.

1. INTRODUCTION

Organic optoelectronic devices are of tremendous and technological interest in photonic applications such as optical interconnection, data link flexible image sensors, and tunable color sensors. Compare to inorganic photodetectors, organic semiconductor (OS) based photodetectors have brought great attention to light detection applications in recent years due to low cost, light-weight, mechanical flexibility, chemical modifications, tunability of absorption range and ease to integrate [1-5]. Generally, Optical Photo-detector (OPD) structure can be separated into the bilayer planer heterostructure where acceptor material is deposited on the donor material and bulk heterostructure, where donor and acceptor materials both are intermixed with each other. The advantage of bilayer structure is that most of the photo-generated carriers are accumulated at the interface between donor and acceptor where dissociated electrons and holes will reduce the recombination of charge carriers at the interface and enable the transport of charge carriers towards their individual electrodes [6-8]. Active layers of phthalocyanine as electron donor and fullerenes as electron acceptor are the most promising materials for organic devices due to high mobility and high absorption range. During last few years, large amount of research works has been published on OPD having a broader spectral range, high-speed, high efficiency, high detectivity, and large dynamic range [9-13]. However, lifetime and speed are also significant problems in the organic electronics industry. To attain high-performance OPD, an understanding of physical processes occurring in an organic semiconductor is essential. Device simulation can provide important information about the operating mechanism in the device and identify the limiting processes. Furthermore, the behavior of OPD can be recognized and performance of OPD can be optimized by using computer-based simulation. The simulation of OPD can be separated into two parts, firstly coupling of light into the device and secondly extraction of the photo-generated carrier from the device.

In this aim, various research works have been undergoing great interest in recent years. Device-level simulations describing the performance of bulk OPD have been demonstrated by different research groups [14-15]. Popescuet. al. used a drift-diffusion simulator from Synopsys to describe the current-voltage characteristics and explored the effects of light intensity on the device parameters [14]. Wurfelet. al. presented the current–voltage curve using same device simulator and studied the impact of charge transport phenomena on that curve [15]. Many research groups reported numerical device modelling describing the current-voltage curve of bulk OPD and studied the effects of different parameters on the device [16-18]. Most of the research activities examined the behavior of the current-

FOREX Publication
Open Access | Rapid and quality publishing
International Journal of Electrical and Electronics Research (IJEER)
Research Article | Volume 10, Issue 4 | Pages 811-816 | e-ISSN: 2347-470X

voltage curve of bulk OPD using numerical simulation tools so far.

In this paper, a bilayer OPD has been simulated which highlights the device-level simulation describing the optoelectrical behavior of the proposed device. The device has been modelled for detailed analysis of the behavior of bilayer OPD. At this point, the drift-diffusion simulator from Synopsys tool has been used for the electrical part along with an optical-generation simulator for the optical part. The simulated current-voltage curve under dark and illumination conditions, photocurrent spectra, and transient response have been studied.

2. MODELLING OF BILAYER ORGANIC PHOTODETECTOR

2.1 Bilayer Organic Photodetector Structure

To investigate the optoelectrical behavior of organic semiconductors, numerical simulation has been performed using the semiconductor device simulation tool TCAD from Synopsys Inc. The Bilayer OPD model was built up by one donor layer with lower electron affinity and acceptor layer with ionized potential. Indium tin oxide and gold were used as electrodes and these were defined by their work function, resistivity, and reflective index. Donor layer and acceptor layers were described by their reflective index, extinction coefficient, bandgap, mobility, and density of states. The energy difference between LUMO of the donor (acceptor) and HOMO of donor (acceptor) was acted as a bandgap of the individual OS. The two OS layers were added between gold and ITO electrodes. The important parameters used to simulate the bilayer OPD are summarized in *table 1*. The device structure of the proposed bilayer model of the OPD is shown in *figure 1 (a)*, in which donor layer and acceptor layer are represented by Copper Phthalocyanine (CuPc) and fullerene (C_{60}). The thickness of CuPc and C_{60} is considered as 50 nm. The energy level diagram of modeled OPD is shown in *figure 1 (b)*.

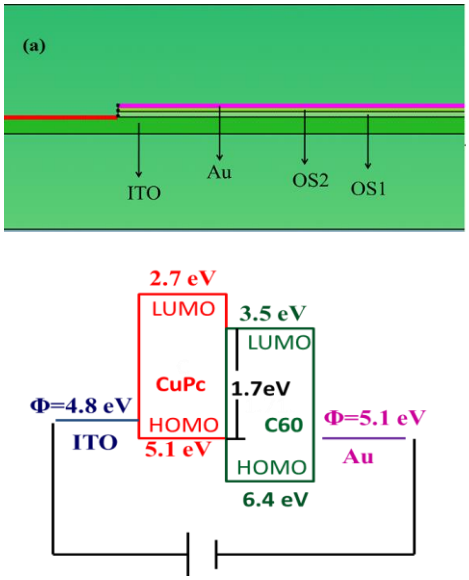

Figure 1: (a) Device structure of bilayer modeled OPD
(b) Energy level diagram of bilayer OPD

Table 1: Bilayer OPD parameters used for simulation

Parameter	Symbol	Value
Band gap of Donor	E_{gos1}	2.4 eV
Band gap of acceptor	E_{gos2}	2.9 eV
Electron affinity of donor	χ_{os1}	2.7 eV
Electron affinity of acceptor	χ_{os2}	3.5 eV
Electron mobility	μ_n	$1.9.10^{-3}$ $cm^2/V.s$
Hole mobility	μ_p	0.3 $cm^2/V.s$
Density of states of donor	N_c	5.10^{18} cm^{-3}
Density of states of acceptor	N_v	5.10^{21} cm^{-3}
Thickness of active layer	t	100nm
Carrier concentration of donor	n_{os1}	10^{15} cm^{-3}
Carrier concentration of acceptor	p_{os2}	10^{18} cm^{-3}
Dielectric constant	ε	7

2.2 Numerical Model

To simulate the OPD electrically and optically, the simulator tool should account for several processes. First, exciton generation, transport, and dissociation, then drift-diffusion of photo-generated carrier and extraction at electrodes should be accountable for the process flow. For exciton generation, an optical-generation model was used in which the rate of exciton generation was assumed to be homogeneous throughout the device [19]. Additionally, physical models of organic semiconductors are required to model reasonably the physical transport processes of organic devices within the framework. These models are the Poole Frenkel Mobility Model, Gaussian Transport Model, Gaussian Density of States model, and Langevin Bimolecular Recombination Model [19]. Poole Frenkel mobility Model is used to model the hopping transport of carriers in OS and that is dependent on the temperature and electric field [16]. The Gaussian Transport Model is used to explain the transport of free carriers and exciton at hetero-interface between two organic layers. The Gaussian density of states approximates the effective density of states for electrons and holes in organic semiconductors [20]. The Langevin Bimolecular Recombination Model is used to explain the recombination process of carriers and the generation process of singlet excitons [16-18]. Electrical simulations have been carried out using a drift-diffusion simulator from Synopsys. This drift-diffusion equation describes the carrier's transport through the device. In the simulation, hole and electron continuity equations were coupled with the Poisson equation. Electron and hole equations are coupled among them through mobility, the density of states, generation, and recombination rate. For computing exciton transport, the singlet exciton equation is used to couple with the Poisson equation.

$$\nabla E = \frac{q}{\varepsilon}(n - p) \quad (1)$$

$$J_n = qn\mu_n E + qD_n \nabla n \quad (2)$$

FOREX Publication
Open Access | Rapid and quality publishing
International Journal of Electrical and Electronics Research (IJEER)
Research Article | Volume 10, Issue 4 | Pages 811-816 | e-ISSN: 2347-470X

$$J_p = qp\mu_p E - qD_p \nabla p \quad (3)$$
$$\frac{\partial n}{\partial t} = \frac{1}{q}\nabla J_n + G_n - R_n \quad (4)$$
$$\frac{\partial p}{\partial t} = \frac{1}{q}\nabla J_p + G_p - R_p \quad (5)$$

Eq. (1) is the Poisson equation where the change of electric field (E) with respect to distance is dependent on the electron (n) and hole densities (p), q is the elementary charge, **ε** is the dielectric constant. Eq. (2) andEq. (3) are the electron and hole current densities equations with the incorporation of drift and diffusion of charge carriers.$\mu_n$and μ_p is the mobility of electron and hole where mobility of organic semiconductor follows Poole-Frenkel-mobility- ($\mu_{n,p}(E) = \mu_{0n,p}\exp(-\frac{E_0}{KT})\exp(\sqrt{E}(\frac{\beta}{300} - \gamma))$).

$D_{n,p}$ is the diffusion coefficient which is given by Einstein equation ($D_{n,p} = \mu_{n,p}K_BT/q$). $G_{n,p}$and$R_{n,p}$ are the generation and recombination rate of free carriers. For modelling the device, carrier concentration profiles were added in two organic semiconductor layers, and then meshing of the profile was defined in the structure in which maximum meshing resolution is 25 nm and dimension of the active area is 100 μm^2. Transport properties of electron and hole have been simulated using the above five equations in the drift-diffusion simulator and the simulated J-V curve, photocurrent spectra, and transient response have been obtained. Absorption photon density and total current density profiles are shown in *figure 2 (a), and (b).*

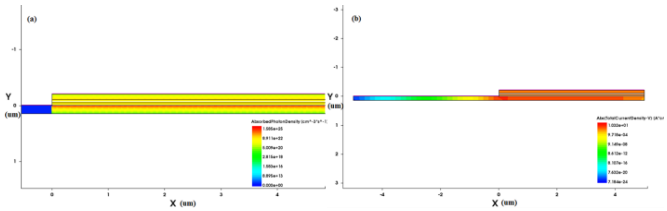

Figure 2: (a) Absorption photon density profile of OPD. (b) Current density profile of OPD

3. RESULTS AND DISCUSSION

3.1 Drift-diffusion Simulation of J-V Curve

The simulated J-V curves under dark condition are illuminated at a wavelength of 600 nm is shown in *figure 3 (a)*. Cathode voltage has been varied between -2 to 0.3 V and a light intensity of 3 W/cm^{2}has been applied. An outstanding rectifying behavior under dark conditions has been observed and the estimated rectification ratio is found to be 104 at ±0.3 V. The observed rectifying behavior is due to the different work functions of electrodes [21]. An optimum value of dark current density is achieved and is found to be 8.56 × 10-9 A/cm^2 at 0 V, as carriers are not easily injected from the electrodes to the active layer due to large barrier height. The result shows less dark current density from the reported dark current curve of Gaoyao et. al [22], where the thickness of CuPc and C_{60} was chosen as 20 nm and 40 nm and the size of the active layer is 3 mm^2. Under illumination condition, device current is observed to increase than in the dark condition that indicates photo-detecting behavior. Under the irradiation of light, generated excitons in the active layer create photo-generated carriers. These carriers are injected by the electrodes without facing large barrier height leads to enhancement of device current. Photocurrent density at 0 V is found to be 6.64 mA/cm^2 under the illumination of 3 W/cm^2 and that photocurrent increases gradually with increases in reverse bias. On the other hand, under forward bias, device current density is observed to increase sharply at 0.3 V due to carrier injection from electrodes [22]. It can be observed that the device offers photocurrent density in μA range under low-intensity light [22-23] whereas in the proposed work, mA range photocurrent density is observed under high-intensity light. Hence, these results suggest that photocurrent density increases with the intensity of light.

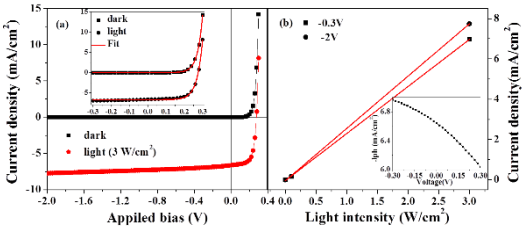

Figure 3: (a) Current vs. voltage curve under dark and illumination conditions. Red lines in inset shows best fitted curve. (b) Photocurrent vs. light intensity curve at -0.3 V and -2 V. Inset shows Photocurrent vs. voltage curve at 3W/cm^2

To describe rectifying behavior of current density-voltage characteristics (J-V curve) of OPD, Shockley equation is used. Relation between J-V curves is governed by *eq. (6)*

$$J = J_0\exp(\frac{qV}{\eta KT}) \quad (6)$$

Where J is the current density, J_0 is the reverse saturation current density in the absence of bias, η is the ideality factor, V is the applied bias, K is the Boltzmann constant, T is the absolute temperature and q is the electronic charge (1.6 × 10^{-19} C). J_0 is related to the Schottky barrier height,$J_o = A * T^2\exp(-q\Phi_B/KT)$, A is the Richardson constant, Φ_B is the barrier height.

Simulated J_{dark}-V curve is fitted with the Shockley *eq.(6)* in which diode current is only dependent on the applied bias. The red-line shown in the inset of *figure 3 (a)* is a fitted curve. From the fitted curve, reverse saturation current density (J_0), barrier height, and ideality factor have been estimated. The estimated barrier height and ideality factor and J_0 are found to be 0.76 eV and 1.05 and 2.45 × 10^{-7} A/cm^2. The estimated J_0 is almost equal to simulated dark current density at 0 V. Ideality factor of 1 in dark condition indicates the dominance of direct (bimolecular) recombination [15, 24-25].

Under illumination, the output current of OPD is operated by two different inputs, one is applied bias and another is incident light (photon flux). Hence to describe illumination current in OPD, one generation current is needed to add in the Shockley equation in which diode current is dependent on the applied bias and generation current is only dependent on the incident light.

$$J = J_0\exp\left(\frac{eV}{\eta KT}\right) - J_{gen} \quad (7)$$

Where J_{gen} is the generation current density.

FOREX Publication
Open Access | Rapid and quality publishing
International Journal of Electrical and Electronics Research (IJEER)
Research Article | Volume 10, Issue 4 | Pages 811-816 | e-ISSN: 2347-470X

The simulated J_{illu}-V curve is fitted using Eq (7) and the red line depicts in *figure 3 (a)* is the fitted curve. From this fitted curve, diode parameters are extracted. J_0 and generation current density (J_{gen}) and ideality factor are found to be 7.968 × 10-7 A/cm^2, 0.0067 A/cm^2 and 1.17. It is observed that under illumination, diode current at low forward bias is activated by the intensity of light. The ideality factor of that diode current deviates from 1 and it is observed to increase slightly from the dark current's ideality factor. The increased in ideality factor under illumination is attributed to the enhancement of recombination. Under forward bias, device current is dependent on the applied bias as well as the intensity of light. Hence, the carrier concentration is increased in the system due to the generation of photo carriers and the injection of carriers from electrodes. At higher carrier concentrations, the recombination rate is increased which indicates the enhancement of ideality factor under illumination [26].

Inset of *figure 3 (b)* shows the simulated photocurrent current curve (extracted from J-V curve) which is observed to decrease strongly with increases in forward bias. We expect that with the application of forward bias, more electrons and holes are injected from electrodes to the active layer and these carriers are recombined with photo-generated carriers [26-27].

In order to obtain a good dynamic range, the linearity of photocurrent response under different intensities is an important parameter for any photodetector. To analyze the linear dynamic range of the OPD, the curve is plotted and is shown in *figure 3* (b). Photocurrent response at -0.3 and -2 V is observed to increase linearly over the intensity of light from 0.1 to 3 W/cm^2. Such linear behavior is found due to the generation of higher excitons with an increase in light intensity. This further indicates that OPD maintains almost constant responsivity with the intensity of light at both reverse bias conditions. From the slope of fitting lines, responsivity at -0.3 and -2 V are found to be 2.3 and 2.5 mA/W respectively. Different values of responsivity at different biases indicate that there is an enhancement of photocurrent. Since with application of the external bias, excitons are easily dissociated into free carriers at the interface and after dissociation, the free carriers are accelerated towards the electrodes within a very small time which leads to the higher photocurrent.

3.2 Photocurrent v/s Wavelength

Photocurrent spectra at different intensities of 0.1 W/cm^2, 3 W/cm^2, and 6 W/cm^2 are shown in *figure 4 (a)*. Most of the photocurrent is observed to be generated in the whole visible region under intensities of 3 W/cm^2 and 6 W/cm^2. Photocurrent produced from 0.55 µm to 0.75 µm is due to photon absorption in the CuPc layer and second photocurrent spectra from 0.35 µm to 0.45µm correspond to photo-absorption of C_{60} layer. An almost equal amount of photocurrent spectra in both spectral regions is attributed to an equal probability of exciton generated and dissociated at the interface between CuPc and C_{60} layers. Almost fifty times less photocurrent is produced in the OPD under the illumination of the intensity of 0.1W/cm^2. Generation of lower photocurrent density under the low intensity can be attributed to less amount of exciton generated in the both OSs which in turn, less photo-generated carrier are generated in the device. Generation of photocurrent is directly proportional to number absorption of incident photon with illumination of light energy. If we apply low intensity of light, less number of electron-hole pairs will be produced as less number of incident photon presented inside the device. Number of incident photon is increased with increment of intensity of light which inturn increases the photocurrent.

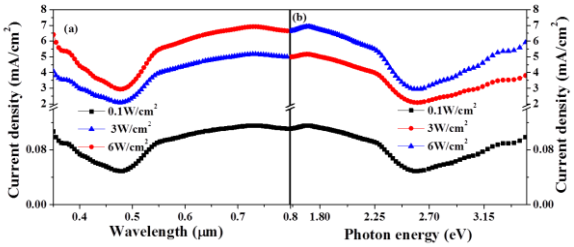

Figure 4: (a) Photocurrent of device vs. wavelength at intensities of 0.1, 3 and 6 W/cm^2. (b)Photocurrent of device vs. photon energy at intensities of 0.1, 3 and 6 W/cm^2

The curve shown in *figure 4 (b)* has been plotted from the photocurrent spectra. In this curve, maximum photocurrent is observed at the photon energy of 1.7 eV. The photon energy corresponds to the difference between the HOMO of the donor and LUMO of the acceptor (effective bandgap energy) [16-18]. Hence it is found that maximum exciton generation occurs in the device when OPD is excited by photon energy corresponds to the effective bandgap energy (at the interface between donor and acceptor material). At 1.7 eV, maximum absorption occurs at the interface indicates the generation of maximum photocurrent due to dissociation of higher probability of exciton at the interface. *figure 5 (a)* represents the responsivity of OPD at intensity of 0.1 W/cm^2, 3 W/cm^2 and 6 W/cm^2 respectively. Responsivity (R) of OPD can be calculated using below formula

$$R = \frac{I_p}{P}$$

where, I_p is photocurrent and P is the incident optical power. The calculated responsively of the proposed model is found to be 1.5 mA/W under the illumination intensity of 3W/cm^2 at zero bias. The proposed responsively is better as compared to responsivity reported in S. Sahu et al [23]. Due to low carrier mobility, charge transport in the system becomes slow and is enhanced by the recombination loss that further indicates the reduction of responsivity [28-29]. On the other hand, the generation of a low probability of exciton in a small active area is responsible for this low responsivity.

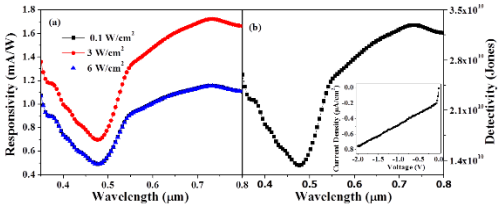

Figure 5: (a) Responsivity vs. wavelength at intensity of 0.1, 3 and 6 W/cm^2.
(b) Detectivity vs. wavelength at intensity of 3 W/cm^2. Inset shows dark current vs. voltage at same intensity

FOREX Publication
Open Access | Rapid and quality publishing
International Journal of Electrical and Electronics Research (IJEER)
Research Article | Volume 10, Issue 4 | Pages 811-816 | e-ISSN: 2347-470X

Different types of noise such as shot noise, Johnson noise, thermal fluctuation noise affect the dissociation efficiency and charge transport efficiency in the device which in turn affects the device performance such as responsivity and detectivity [30-31]. The inset of *figure 5 (b)* depicts the dark current density-voltage curve. Dark current density is observed to be 8.56 nA/cm^2 at 0 V and it is increased about to two orders when a reverse bias is ramped from 0 to -2 V. Shot noise is the major contribution for the dark current density which correspondingly limits the device detectivity. The specific detectivity is another important parameter for determining the noise performance of photodetector and it can be measured using the below formula,

$$D^* = \frac{R}{(2qJ_d)^{1/2}}$$

where R is responsivity and J_d is the dark current density and q is the electron charge (1.6×10^{-19}C). The calculated result of specific detectivity under a light intensity of 3 W/cm^2 is shown in *figure 4 (b)*. The detectivity is found to be 3×10^{10} Jones at 650 nm and zero bias. Due to the high dark current, detectivity is obtained in the order of 10^{10}. A similar order of detectivity has been found in another report but in that case, light source having a wavelength of 900 nm was used [22]. Another main reason for the low detectivity is attributed to the injection of electron (hole) from the anode (cathode) to the active layer under reverse bias condition [32]. Transient curves of modelled OPD at pulse periods of 1s and 2s under different bias conditions are shown in *figure 6 (a)* and *figure 6 (b)* respectively. From both figures, similar and clear photo-response behaviors are observed at 0 V and -5 V. With the illumination of light on and off, device current shows two different states, a low state with the magnitude of 5.25 nA in the dark and a high state with a magnitude of 6.96 nA at a light intensity of 3 W/cm^2 and -5 V. The ratio of photocurrent to dark current at -5 V and is found to be 1.32 under intensity 3 W/cm^2.

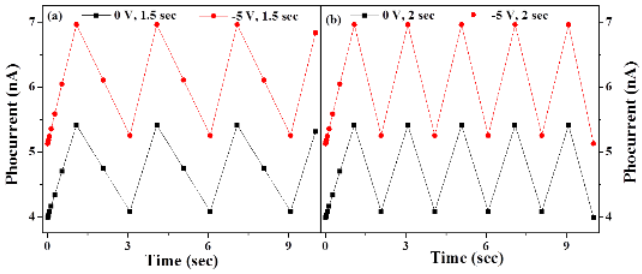

Figure 6: Simulated transient response at 0V and -5V under pulse period of (a) 1.5 second and (b) 2 second

Moreover, same shape of pulse photo-response is obtained for the illumination pulse period of 1.5 (repetition frequency 600 MHz) and 2 s (repetition frequency 500 MHz) in *figure 6*. Due to the presence of interface trap density at the interface, the majority of photo-generated carriers got loss (detained) before reaching the respective electrodes. Additionally, due to the large transport distance, low mobility carriers yield a long time to collect by the electrodes. These two processes limit the response speed of OPD [33-35].

In transient response, it is observed, the device is not responding properly for pulse widths of 1.5 s and 2 s. Output current saturates to its maximum value (6.64 nA at 0V) after 1.5 s. Using Eq. (8), the saturation time/rise time is calculated.

$$I = I_0(1 - e^{-\alpha t}) \quad (8)$$
$$I = I_0 e^{-\alpha t} \quad (9)$$

Where I is the photocurrent and I_0 is the saturation value of photocurrent. Using Eq. (8), a curve is plotted in *figure 7* and the value of α has been estimated. The inverse value of α determines the time constant of the device due to light shining on OPD and is noted as 5 s. Hence, the response time of the device is 5 s.

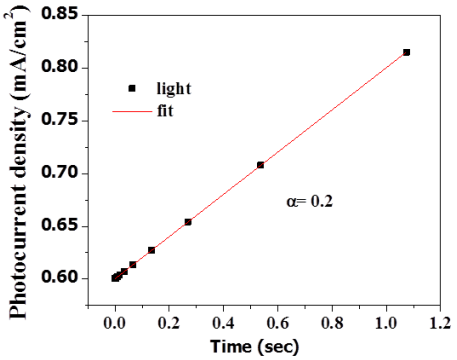

Figure 7: I/I_0 Vs Time at 0 V

Fall time of the OPD has been calculated using Eq. (9) and the value is found to be 10 s. The reason for different rise time and fall time is due to the influence of a localized coulomb force which works between electron and hole [11]. Response time also provides the depletion capacitance and depletion width of the OPD. The depletion capacitance ($C=\tau/R$, where τ is the time constant and R is the differentiate resistance) and width ($W=\varepsilon A/d$) are found to be 116 nF and 0.0053 nm. Comparison of previous photodetector with present photodetector is shown in *table 2*.

Table 2: Comparison of previous photodetector with present photodetector

Structure	Photocurrent (A)	Dark current (A)	Responsivity (A/W)	Ref
ZnO:rGO	10 x 10^{-9}	2 x 10^{-9}		[36]
PEDOT:PSS/ pentacene/ F_{16}CuPc	21.3 x 10^{-6}	2 x 10^{-6}	2.9 x 10^{-3}	[37]
CuPc/C60	6 x 10^{-3}	Order of 10^{-9}	1.6 x 10^{-3}	Present work

4. CONCLUSION

In conclusion, the modelling of organic photodetector based on bilayer structure has been reported. Drift-diffusion simulator and optical-generation simulator from Synopsys tool have been incorporated and the optoelectronic behavior of OPD has been analyzed. OPD shows good rectifying behavior under dark condition due to the different work functions of electrodes. The

FOREX Publication
Open Access | Rapid and quality publishing
International Journal of Electrical and Electronics Research (IJEER)
Research Article | Volume 10, Issue 4 | Pages 811-816 | e-ISSN: 2347-470X

photocurrent density of 6.64 mA/cm^2 has been observed under the illumination of 3 W/cm^2 and the photocurrent is increased gradually with increases in reverse bias. To describe rectifying behavior of current density-voltage characteristics of OPD, the curve has been fitted using the Shockley equation. Under application of forward bias, the deviation of the ideality factor of diode current deviates from 1 under illumination from that of dark current which indicates enhancement of recombination loss due to generation of photo-carrier and injection of carriers. Generation of equal probability of photocurrent spectra in whole spectral region attributes to the equal probability of exciton generated and dissociated at the interface between CuPc and C_{60} layers. Specific detectivity of the proposed device is in the order of 10^{10} Jones at 650 nm due to the high dark current density and the recombination loss occurring in the device. The presence of interface trap density and the large transport distance are responsible for optimum response speed in OPD.

REFERENCES

[1] Peumans, P., Yakimov, A., Forrest, S. R., (2004). Appl. Phys. 95 (93), 2938.

[2] Schilinsky, P., Waldauf, C., Hauch, J., et al. (2004). Thin Solid Films. 451, 105–108.

[3] Wang, J. B., Li, W. L., Chu, B., et al (2011). Org. Electron. 12, 34.

[4] Yang, D., Zhou, X., Ma, D., (2013) .Org. Electron. 14(11), 3019.

[5] Baeg, K. J., Binda, M., Natali, D., et al. (2013). Adv. Mater. 25, 4267–4295.

[6] Coakley, K. M., McGehee, M. D., (2004). Chem Mater.16, 4533-4542.

[7] Benanti, T. L., Venkataraman, D., (2006). Photosynth Res. 87, 73-81.

[8] Günes, S., Neugebauer, H., Sariciftci.Chem N.S., (2007). Rev.107, 1324-1338.

[9] Clark J., (2010). Lanzani. Nat G., Photonics 4, 438.

[10] Wei, G., Lu, Z., Cai, Y., (2017). et al. Mater. Lett.201, 137–139.

[11] Morimune, T., Kajii H., Ohmori, Y., (2006). IEEE Photon. Technol. Lett. 18(24), 2662-2664.

[12] Zimmerman, J. D., Diev, V. Y., Hanson, K., Lunt R, R., et. al. (2010). Adv. Mater. 22, 2780.

[13] Tsai, W. W., Chao, Y. C., Chen, E. C., et al. (2009). Appl. Phys. Lett. 95, 213308.

[14] Popescu, B. V., Popescu, D. H., Lugli, P., et al. (2013). IEEE Trans. Electron Devices 60(6), 1975.

[15] Wurfel, U., Neher, D., Spies A., et al (2015). Nat. Commun. 6, Article number: 6951.

[16] Christ N. S., Kettlitz, S. W., Valouch, S., et al (20090 J. Appl. Phys. 105, 194513.

[17] Koster, L. J. A., Smits E.C.P., et al. (2005). Phys. Rev. B 72, 085205.

[18] Hausermann R., knapp, E., Moos M., et al. (2009). J. Appl. Phys. 106, 104507.

[19] Synopsis (2013).TCAD Sentaurus: Sentaurus Device User Guide; Release H-2013.03.

[20] Torricelli F., Colalongo, L., (2009). IEEE Electron.Devices Lett.30(10), 1048.

[21] Hu, L., Iwasaki A., Suizu, R., et al. (2011). Phys. Rev. B 84, 205329.

[22] Wei, G., Lu, Z., Cai Y., et al. (2017).Mater. Lett.201, 137–139.

[23] Sahu, S., Pal, A. J., Nanosci, J., (2009). Nanotechnol.9, 450–454.

[24] Hawks, S.A., Li, G., Yang, Y., et al. (2014). J. Appl. Phys. 116, 074503.

[25] Jan, G., Wetzelaer, A. H., Blom, P. W. M., (2014). NPG Asia Mater.6, e110.

[26] Wang,Z., Cheng,Z., Delahoy, A.E., et al. (2013). IEEE J. Photovolt. 3(2).843-851.

[27] Osasa, T., Yamamoto S., Matsumura, M., (2006). Jpn. J. Appl. Phys. 45(4B), 3762–3765.

[28] Mandoc, M. M., Veurman, W., Koster, L. J. A., et al. (2007). Adv. Funct. Mater.17, 2167–2173.

[29] Mudhaffera, M. F. A., Griffitha, M. J., Feron, K., et al. (2017). Sol. Energy Mater Sol. Cells. 175, 77–88.

[30] Armin, A., Vuuren, R. D. J., Kopidakis, N., et al (2015). Nat. Commun.6, 1–8.

[31] Wu, Z.H., Yao, W. C., Alexander, E. L., et al. (2017). ACS Appl. Mater. Interfaces 9, 1654-1660.

[32] Wang, Y., Yang, D., Zhou, X., et al. (2017). Org. Electron. 42, 203-208.

[33] Pivrikas, A., Neugebauer, H., Sariciftci N.S., (2010). IEEE.J. Sel. Topics Quantum Electron.16(6), 1746-1758

[34] Arca, F., Tedde, F., Sramek, M., et. al. (2013). Sci. Rep. 3, Article number: 1324

[35] Ahmada,. Suhailb, M.H., Muhammad I.I., (2013). et. al. Chin.Phys. B. 22(10), 100701.

[36] Nath, D., Mandal, S. K., Deb, D., Rakshit, J. K., Dey,P., Roy, J. N., (2018). J. Appl. Phys.123, 095115.

[37] Nath, D., Dey, P., Joseph, A. M., Rakshit, J. K., Roy, J. N., (2020) J. Alloys Compd. 815 152401.